STRUCTURAL CHEMISTRY
ISSN 2053-2296

'NMR Crystallization': *in-situ* NMR techniques for time-resolved monitoring of crystallization processes

Kenneth D. M. Harris,* Colan E. Hughes, P. Andrew Williams and Gregory R. Edwards-Gau

School of Chemistry, Cardiff University, Park Place, Cardiff CF10 3AT, Wales. *Correspondence e-mail: harriskdm@cardiff.ac.uk

Received 23 November 2016
Accepted 12 December 2016

Edited by D. Bryce, University of Ottawa, Canada

Keywords: NMR crystallography; *in-situ* NMR; CLASSIC NMR; time-resolved; crystallization processes.

Solid-state NMR spectroscopy is a well-established and versatile technique for studying the structural and dynamic properties of solids, and there is considerable potential to exploit the power and versatility of solid-state NMR for *in-situ* studies of chemical processes. However, a number of technical challenges are associated with adapting this technique for *in-situ* studies, depending on the process of interest. Recently, an *in-situ* solid-state NMR strategy for monitoring the evolution of crystallization processes has been developed and has proven to be a promising approach for identifying the sequence of distinct solid forms present as a function of time during crystallization from solution, and for the discovery of new polymorphs. The latest development of this technique, called 'CLASSIC' NMR, allows the simultaneous measurement of *both* liquid-state *and* solid-state NMR spectra as a function of time, thus yielding complementary information on the evolution of both the liquid phase and the solid phase during crystallization from solution. This article gives an overview of the range of NMR strategies that are currently available for *in-situ* studies of crystallization processes, with examples of applications that highlight the potential of these strategies to deepen our understanding of crystallization phenomena.

1. Introduction

Among the wide range of experimental techniques for studying solid materials, solid-state NMR spectroscopy (Duer, 2004; Apperley *et al.*, 2012) stands out as one of the most versatile, due to the wide variety of different types of knowledge that can be obtained, including information on local structural properties, internuclear interactions and dynamic processes. Furthermore, as each NMR-active isotope has a unique set of NMR properties, studies of different nuclei within the same material have the potential to yield a vast amount of complementary information about the structural and dynamic properties of the material.

However, although solid-state NMR is a powerful technique for characterization of the structural and dynamic properties of solids, adapting the technique for *in-situ* studies of chemical processes is associated with technical challenges, including the fact that high-resolution solid-state NMR spectra are usually recorded with the sample sealed inside a rotor undergoing rapid magic-angle spinning (at frequencies typically around 10 kHz) in a confined and relatively inaccessible space inside the magnet of the NMR spectrometer. Consequently, the development of *in-situ* solid-state NMR techniques has generally lagged behind advances made in other *in-situ* experimental strategies, such as those based on

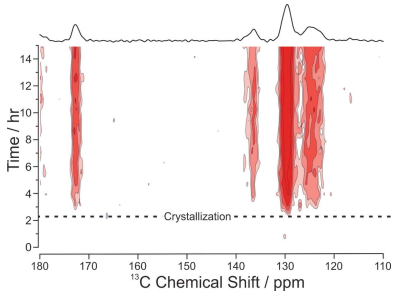

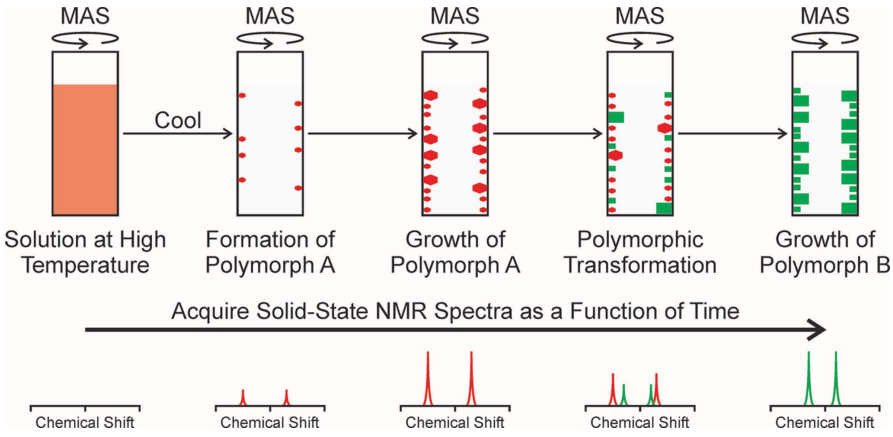

Figure 1
Schematic of the strategy for *in-situ* solid-state NMR studies of crystallization processes, illustrated by the case of a system in which the crystallization process initially produces a metastable polymorph *A* (red), followed by a transformation to produce a more stable polymorph *B* (green). The corresponding changes in the measured solid-state NMR spectrum as a function of time are shown in the lower part of the figure.

diffraction, microscopy and other spectroscopies. Furthermore, *in-situ* solid-state NMR studies of crystallization from the solution phase pose additional challenges, particularly as the experimental set-up must ensure that the liquid phase remains properly sealed within the NMR rotor, even under conditions of rapid magic-angle spinning.

As highlighted in this article, we have recently been motivated to explore the opportunities for developing *in-situ* solid-state NMR strategies to investigate the evolution of crystallization processes, recognizing that crystal growth (Kahr & McBride, 1992; RSC, 2007) is crucially important in many aspects of pharmaceuticals, materials, chemical and biological sciences. Clearly, an improved fundamental understanding of crystallization systems has important practical applications (such as enabling greater control of the outcome of crystallization processes in industrial contexts). New experimental strategies are undoubtedly crucial in allowing a deeper physicochemical understanding of crystallization to be achieved, and techniques that allow direct *in-situ* monitoring of the process have a particularly important role to play in this regard.

In general, crystallization processes are governed by kinetic factors, with metastable polymorphs often produced rather than the thermodynamically stable polymorph. In this context, polymorphs (Dunitz, 1991; Bernstein, 2002, 2005; Davey, 2003; Chen *et al.*, 2005; Ahn *et al.*, 2006; Harris, 2006; Price, 2008) are defined as crystalline materials with identical chemical composition but different crystal structures. Crystallization processes often evolve through a well-defined sequence of distinct solid forms, before the final crystallization product is reached, although details of the time-evolution of the process can depend critically on the exact conditions of the experiment. To optimize and control such crystallization processes, it is essential to understand the sequence of events involved, rather than simply characterizing and identifying the final crystalline product. To achieve this aim, experimental strategies that allow direct *in-situ* monitoring of crystallization processes are clearly essential.

Several different *in-situ* techniques have been used to study crystallization processes (Pienack & Bensch, 2011), including scattering techniques [*e.g.* X-ray diffraction (either in energy-dispersive or angular-dispersive mode), small-angle X-ray scattering, neutron diffraction and small-angle neutron scattering], spectroscopic methods (*e.g.* IR, Raman or X-ray absorption spectroscopies) and microscopy (*e.g.* atomic force microscopy and transmission electron microscopy). However, until recently, solid-state NMR spectroscopy had not been utilized in this regard, as a consequence of the technical challenges discussed above.

In recent years, we have developed new *in-situ* solid-state NMR strategies (Hughes & Harris, 2008, 2010) for monitoring the evolution of the solid phase during crystallization from solution. These strategies have the potential to yield new insights into several aspects of crystallization processes, particularly regarding the evolution of different polymorphic forms (and interconversion between polymorphs) as a function of time. Most recently (Hughes *et al.*, 2014), we further extended the methodology by proposing and demonstrating a strategy for *in-situ* studies of crystallization involving the simultaneous measurement of both liquid-state and solid-state NMR data, allowing the evolution of both the solid phase and the liquid phase to be probed as a function of time during the same crystallization experiment. This technique is called CLASSIC NMR (Combined Liquid- And Solid-State In-situ Crystallization NMR). We describe the basis of the CLASSIC NMR strategy and give representative examples of the application of this technique. Finally, for crystallization systems in which the rate of crystallization is significantly more rapid than the time required to record an individual solid-state NMR spectrum (*e.g.* due to long spin-lattice relaxation times for the solid phase), *in-situ* solid-state NMR may not be a feasible approach for probing the time-evolution of the crystallization process. Nevertheless, *in-situ* liquid-state NMR studies can still yield significant understanding of certain aspects of crystallization behaviour, and we also discuss the prospects and opportunities for using *in-situ* liquid-state NMR under these circumstances.

This article presents an overview of recent developments in all these aspects of the *in-situ* monitoring of crystallization

processes using NMR techniques. Given the progress that these techniques have established in revealing new insights into crystallization phenomena, this area of scientific investigation – *NMR Crystallization* – may be identified as a sub-discipline within the burgeoning field of *NMR Crystallography*.

2. Experimental aspects of *in-situ* solid-state NMR studies of crystallization

The ability of high-resolution solid-state NMR to distinguish between different solid forms of a given molecule (*e.g.* polymorphs, hydrates, solvates, cocrystals, *etc.*) is well established (Balimann *et al.*, 1981; Harris & Thomas, 1991; Harris, 2006). For organic materials, different solid forms give rise to distinct high-resolution solid-state ^{13}C NMR spectra, which are often recorded using the technique of ^{1}H$\rightarrow$^{13}C cross polarization (CP) (Duer, 2004; Apperley *et al.*, 2012), together with magic-angle sample spinning (MAS; typical spinning frequencies *ca* 10 kHz) and high-power ^{1}H decoupling. The ^{1}H$\rightarrow$^{13}C CP technique has the advantage of enhanced signal intensity compared to direct excitation of the ^{13}C nuclei. Solid-state ^{31}P NMR is also an attractive proposition due to the fact that the natural isotopic abundance of ^{31}P is 100% (for comparison, the natural isotopic abundance of ^{13}C is only 1.1%). For *in-situ* studies of crystallization from solution, the CP technique has the additional major advantage (Hughes & Harris, 2008) that, under normal conditions, CP measurements on a heterogeneous liquid/solid sample give a signal *only* for the solid component, thus allowing the *selective* detection of the solid phase in crystallization systems (with the dissolved solute and solvent rendered 'invisible' to the measurement).[1] In contrast, X-ray or neutron scattering techniques applied to the same system would give rise to scattering both from the crystalline solid particles (giving rise to Bragg diffraction peaks) and from the solution phase (giving rise to a broad background scattering).

While solid-state NMR spectra cannot, in general, be recorded on a standard liquid-state NMR instrument, it is possible to record liquid-state NMR spectra of reasonable quality on a dedicated solid-state NMR instrument (although the resolution is generally compromised in comparison to spectra recorded on a dedicated liquid-state NMR spectrometer). Using a direct-excitation pulse sequence on a heterogeneous liquid/solid system (*e.g.* a crystallizing system), the NMR spectrum generally contains contributions from both the liquid state and the solid state, although the liquid component typically gives much sharper lines and can thus be readily identified. Moreover, the selective measurement of *only* the liquid-state NMR spectrum can be achieved using direct excitation measurements with a sufficiently short recycle delay (provided the spin-lattice relaxation time for the solid component is not unusually short). Thus, using a solid-state NMR spectrometer, measurements on heterogeneous liquid/solid systems can be set up such that either the solid-state NMR spectrum is observed selectively or the liquid-state NMR spectrum is observed selectively. This feature is critical to the success of the CLASSIC NMR technique discussed in §4.

Until recently, the prospect of using solid-state NMR for *in-situ* studies of crystallization from solution was limited by the difficulty of sealing a liquid phase or a heterogeneous liquid/solid system inside an NMR rotor such that MAS can be carried out at several kHz without the liquid leaking from the rotor. In recent years, suitable rotor technology has been developed to allow liquid samples to be sealed inside NMR rotors for MAS experiments. This technical development paved the way for the types of experiment described here.

In our *in-situ* solid-state NMR strategy for monitoring crystallization processes (shown schematically in Fig. 1), we first prepare a homogeneous (undersaturated) solution inside the NMR rotor at high temperature and then cool the sample to a specific target temperature at which the solution is supersaturated, thereby inducing crystallization. High-resolution solid-state NMR spectra are recorded repeatedly as a function of time to monitor the time-evolution of the solid phase during the crystallization process. The time-resolution of the technique clearly depends on the time required to record an individual NMR spectrum of adequate quality to identify and distinguish the different solid forms present at different stages during the process.

Clearly, it is desirable to be able to detect and identify the very first solid particles produced in the crystallization process, at which stage the amount of solid in the system is generally very low. Thus, optimizing the sensitivity of the measurement is important in allowing solid-state NMR spectra of adequate quality to be recorded in the shortest possible time. To maximize the sensitivity, isotopic labelling of the material to be crystallized is desirable when studying nuclei of low natural abundance (*e.g.* ^{13}C) and carrying out the experiment at high magnetic field is also clearly advantageous. Consequently, much of our research in this field is carried out at the UK National High-Field (850 MHz) Solid-State NMR Facility.

3. *In-situ* solid-state NMR studies of crystallization processes

3.1. Polymorphic evolution during crystallization

The first applications of the *in-situ* solid-state NMR strategy focused on crystallization of glycine ($H_3^+NCH_2CO_2^-$) from different solvents. Crystallization of glycine has been very widely studied (Albrecht & Corey, 1939; Iitaka, 1960, 1961; Jönsson & Kvick, 1972; Kvick *et al.*, 1980; Garetz *et al.*, 2002; Drebushchak, Boldyreva, Drebushchak & Shutova, 2002; Drebushchak, Boldyreva & Shutova, 2002; Ferrari *et al.*, 2002;

[1] We note that, in principle, the NMR signal recorded under CP conditions may also contain a contribution from solute molecules involved in dynamic exchange between the surfaces of the growing crystals and the solution phase. However, such exchanging molecules are expected to give rise to a detectable contribution to the CP NMR spectrum only if the rate of exchange is in an appropriate regime and only if the number of exchanging molecules is not insignificant relative to the number of molecules in the crystalline phase. The latter requirement is likely to be satisfied only in the early stages of the crystallization process when the size of the crystalline particles is very small.

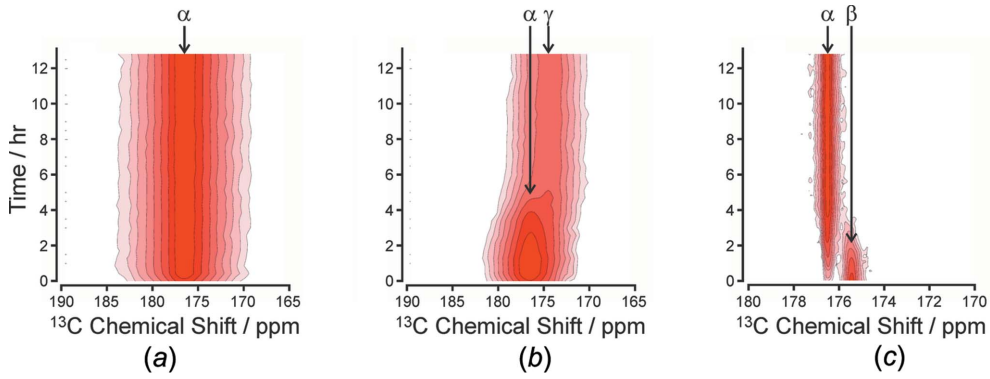

Figure 2
In-situ $^{1}H \rightarrow {}^{13}C$ CP NMR spectra of glycine crystallizing from (*a*) H_2O, (*b*) D_2O and (*c*) H_2O/methanol. Only the carboxylate region is shown. The known peak positions for the α, β and γ polymorphs are indicated. In each case, intensity contour intervals are defined on a logarithmic scale.

Boldyreva *et al.*, 2003; Towler *et al.*, 2004; Taylor, 2004; Weissbuch *et al.*, 2005; Xu & Harris, 2007; Hughes *et al.*, 2007; Poornachary *et al.*, 2007; Hamad *et al.*, 2008; Hughes & Harris, 2009; Chen *et al.*, 2011; Han *et al.*, 2013) and has acquired the status of a prototypical system in polymorphism research. Three polymorphs of glycine (denoted α, β and γ) are known under ambient conditions (Albrecht & Corey, 1939; Iitaka, 1960, 1961; Jönsson & Kvick, 1972; Kvick *et al.*, 1980). The γ polymorph is thermodynamically stable, while the β polymorph is the least stable form (Perlovich *et al.*, 2001; Boldyreva *et al.*, 2003). According to the literature, the metastable α polymorph is the product usually obtained by crystallization from water at neutral pH. However, an early publication (Iitaka, 1961) suggested that crystallization from deuterated water may promote the formation of the γ polymorph, although systematic studies of this isotope effect were only reported recently (Hughes *et al.*, 2007; Hughes & Harris, 2009), in which it was demonstrated that deuteration (even at levels as low as 1%) does significantly increase the probability of obtaining the γ polymorph as the final crystallization product. The polymorphs of glycine are readily distinguished by high-resolution solid-state ^{13}C NMR, as the isotropic peaks for the carboxylate group (Taylor, 2004) are sufficiently well resolved (176.5, 175.5 and 174.5 ppm for the α, β and γ polymorphs, respectively).

The application of the *in-situ* solid-state NMR strategy (Hughes & Harris, 2008) to study crystallization of doubly ^{13}C-labelled glycine ($H_3{}^{+}N{}^{13}CH_2{}^{13}CO_2{}^{-}$) from water with natural isotopic abundances, using time-resolved $^{1}H \rightarrow {}^{13}C$ CP NMR measurements, is shown in Fig. 2(*a*). At the earliest stages of crystallization, a peak emerges at 176.5 ppm and continues to grow as a function of time. From the ^{13}C chemical shift, this solid phase is assigned as the α polymorph, indicating that formation and growth of the α polymorph occurs under these conditions, with no detectable amounts of the β or γ polymorphs throughout the 13 h duration of the experiment.

A separate *in-situ* solid-state NMR experiment (Fig. 2*b*) investigated the crystallization of doubly ^{13}C-labelled glycine from deuterated water. In this experiment, the total level of deuteration for all exchangeable H-atom sites in the system was 86%. Again, the α polymorph is the first solid form produced, suggesting that the same nucleation pathway is followed in both the deuterated system and in the system with natural isotopic abundances discussed above. The amount of the α polymorph continues to increase during the first 1.5 h of the crystallization experiment, but then a new peak emerges at 174.5 ppm, characteristic of the γ polymorph. The intensity of the new peak then increases as a function of time, with a concomitant decrease in the intensity of the peak due to the α polymorph. There is no evidence that the transformation from the α polymorph to the γ polymorph proceeds through any intermediate solid phase, consistent with the rate of increase in the amount of the γ polymorph mirroring the rate of decrease in the amount of the α polymorph. Throughout the period after *ca* 1.5 h, the total amount of solid glycine remains approximately constant. As dry powder samples of the α polymorph under ambient conditions do not transform to the γ polymorph on the timescale observed in the *in-situ* solid-state NMR study, the polymorphic transformation in D_2O can be assigned as a solution-mediated process (rather than a direct solid-to-solid transformation). For both isotopomeric systems, the final form of glycine obtained is consistent with the preferred polymorphic outcome observed in *ex-situ* laboratory crystallization experiments (Hughes & Harris, 2009) carried out under the same conditions and over the same total period of time.

Another *in-situ* solid-state NMR study (Hughes & Harris, 2010) explored the crystallization of glycine from a mixed methanol/water solvent, which has been reported (Weissbuch *et al.*, 2005) to promote the formation of the β polymorph. The *in-situ* solid-state ^{13}C NMR spectra recorded as a function of time are shown in Fig. 2(*c*). In these experiments, the glycine molecules were ^{13}C-labelled only in the carboxylate group (*i.e.* $H_3{}^{+}NCH_2{}^{13}CO_2{}^{-}$), eliminating the line broadening due to unresolved $^{13}C\cdots{}^{13}C$ *J*-coupling in the doubly ^{13}C-labelled glycine used in the studies shown in Figs. 2(*a*) and 2(*b*) and hence giving significantly narrower peaks. In the first spectrum recorded, the solid phase is identified as an almost pure sample of the β polymorph of glycine, together with a very small amount of the α polymorph. The β polymorph is then observed to transform to the α polymorph over a period of *ca* 4 h, again by a solution-mediated transformation. Importantly, the results establish the timescale of the polymorphic transformation and indicate that a viable strategy for isolating an

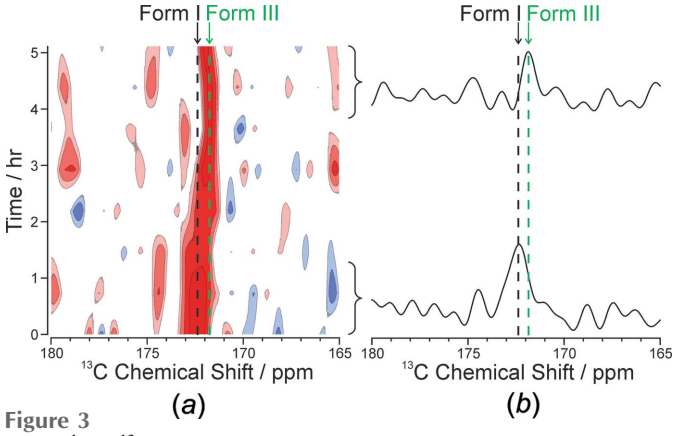

Figure 3
In-situ ^{1}H→^{13}C CP NMR spectra recorded as a function of time during the crystallization of *m*-ABA from methanol, showing the region of the spectrum containing the peak for the carboxylate group. The known peak positions for the carboxylate groups in Forms I and III are highlighted by dashed lines. (*a*) The intensity contour plot showing all spectra recorded as a function of time during the *in-situ* study [intensity contour intervals are defined on a logarithmic scale, with the same scale used both for contours of positive intensity (red shades) and contours of negative intensity (blue shades)]. (*b*) Summation of the first two spectra (bottom) and the last two spectra (top) recorded during the *in-situ* study.

essentially pure sample of the β polymorph would be to stop the crystallization experiment at the stage of the initial solid product, within only a few minutes of triggering the crystallization process.

Another example of polymorphic evolution during crystallization is observed in the crystallization of *m*-aminobenzoic acid (*m*-ABA) from methanol. To date, five polymorphs of *m*-ABA are known (Théorêt, 1971; Williams *et al.*, 2012), and the crystal structures of four polymorphs (Forms II, III, IV and V) have been reported (Voogd *et al.*, 1980; Williams *et al.*, 2012). From a combination of experimental techniques, including N(1s) X-ray photoelectron spectroscopy (XPS), it is known that Forms I, III and IV contain zwitterionic *m*-ABA molecules, whereas Forms II and V contain nonzwitterionic *m*-ABA molecules. Each polymorph is uniquely distinguished by high-resolution solid-state ^{13}C NMR (Hughes *et al.*, 2014), which enables the polymorphs present during *in-situ* crystallization experiments to be identified readily. Results from the *in-situ* solid-state ^{13}C NMR study of crystallization of *m*-ABA from methanol are shown in Fig. 3. From peak assignments, the first solid form produced during crystallization of *m*-ABA from methanol is Form I (black dashed line). Subsequently, a polymorphic transformation occurs to produce Form III (green dashed line), and by *ca* 9 h from the start of the experiment, the crystallization product is a monophasic sample of Form III. As the thermodynamically stable polymorph of *m*-ABA under ambient conditions is Form III, no further polymorphic evolution during the crystallization experiment is expected or observed.

3.2. Discovery of new polymorphs

The *in-situ* solid-state NMR studies discussed in §3.1 demonstrate the capability of the technique to observe and identify intermediate solid forms produced during crystallization in cases for which the transient polymorphs were already known and well characterized. Clearly, the same strategy has the potential to reveal the existence of previously unknown solid forms that exist as transient phases during crystallization (Hughes *et al.*, 2012). In such cases, *in-situ* solid-state NMR studies furnish insights into the specific crystallization parameters required to produce the new solid form(s) and establish the specific 'time-window' during which each new solid form is present in the crystallization system.

As an example, we consider the family of hydrogen-bonded cocrystals formed between even-chain α,ω-dihydroxyalkanes and urea (in a 1:2 molar ratio). These cocrystals have been reported previously (Martí-Rujas *et al.*, 2011) for α,ω-dihydroxyalkanes, $HO(CH_2)_nOH$, with n = 6, 8, 10, 12, 14 and 16. The crystal structures contain double-stranded hydrogen-bonded ribbons of urea molecules; adjacent ribbons are linked by hydrogen bonding to the α,ω-dihydroxyalkane molecules, resulting in a ladder-like arrangement. The observed crystal structures can be subdivided into three well-defined structure types characterized by the following features: (i) the two strands of the hydrogen-bonded urea ribbon are either *parallel* or *antiparallel*, and (ii) the angle between the axis of the α,ω-dihydroxyalkane molecule and the positive direction of the urea strand is either *acute* or *obtuse*. An extensive study of crystallization of these materials *from solution* (using a wide range of different crystallization conditions and solvents) led to the conclusion that each α,ω-dihydroxyalkane forms only one type of cocrystal with urea in solution-state crystallization experiments, with no polymorphism observed for any member of the family.[2] Thus, 1,6-dihydroxyhexane–$(urea)_2$ was found only in the *antiparallel*/*acute* structure type, 1,8-dihydroxyoctane–$(urea)_2$ was found only in the *parallel*/*acute* structure type and 1,10-dihydroxydecane–$(urea)_2$ (and all cocrystals with longer α,ω-dihydroxyalkanes) was found only in the *antiparallel*/*obtuse* structure type. In order to explore the possibility that other solid forms within the α,ω-dihydroxyalkane–$(urea)_2$ cocrystal system may exist on the pathway towards crystallization of these 'preferred' polymorphs, an *in-situ* solid-state NMR study was carried out (Hughes *et al.*, 2012).

We focus on the results from the *in-situ* solid-state ^{13}C NMR study of the crystallization of urea and 1,10-dihydroxydecane from methanol, carried out under conditions known to promote the formation of the 1:2 cocrystal [rather than the formation of the conventional urea inclusion compound (Fetterly, 1964; Harris, 1993, 1996, 1997, 2007; Guillaume, 1999; Hollingsworth, 2002), in which 1,10-dihydroxydecane molecules are included as 'guests' inside the one-dimensional tunnels in the well-known urea 'host' tunnel structure]. Using ^{13}C-labelled urea to enhance the sensitivity of the measurement, the time-resolution of the *in-situ* study (dictated by the

[2] A subsequent study (Zhou *et al.*, 2015) showed that polymorphs of cocrystals within this family can be obtained using mechanochemical techniques. Specifically, for both 1,6-dihydroxyhexane–$(urea)_2$ and 1,8-dihydroxyoctane–$(urea)_2$, polymorphs with the *antiparallel*/*obtuse* structure type were obtained.

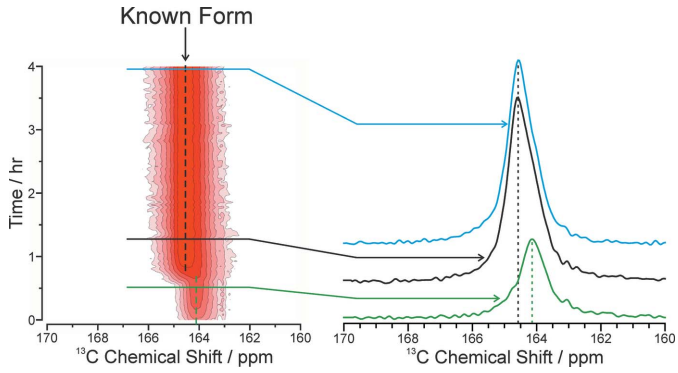

Figure 4
In-situ ^{1}H→^{13}C CP NMR spectra (showing the spectral region containing the urea peak) recorded as a function of time during crystallization of 1,10-dihydroxydecane and ^{13}C-labelled urea from methanol. Intensity contour intervals are defined on a logarithmic scale.

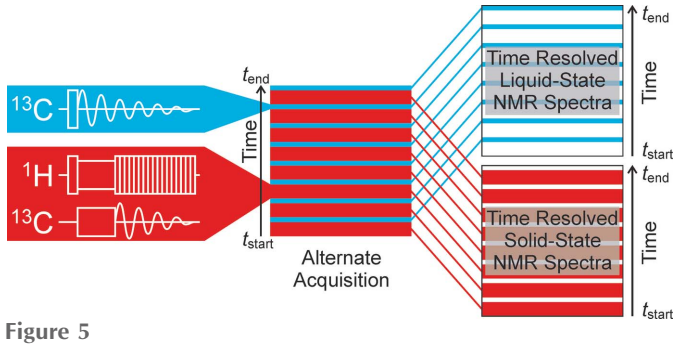

Figure 5
Schematic of the CLASSIC NMR experiment, in which *in-situ* NMR spectra are recorded as a function of time during crystallization using two alternating pulse sequences. One pulse sequence (red) detects the solid phase selectively and the other pulse sequence (blue) detects the liquid phase selectively. After completing the experiment, the two sets of data are separated to give a time-resolved set of solid-state NMR spectra (red) and a time-resolved set of liquid-state NMR spectra (blue).

time taken to record a single solid-state ^{13}C NMR spectrum) was 2.67 min.

The results of the *in-situ* solid-state ^{13}C NMR study are shown in Fig. 4, focusing on the region of the spectrum containing the ^{13}C peak for urea. The first recorded spectrum has a single isotropic peak at 164.12 ppm, which grows in intensity over the next 40 min. At this time, a new peak at 164.58 ppm appears suddenly and then grows rapidly in intensity. The new peak corresponds to the known 1,10-dihydroxydecane–(urea)$_2$ cocrystal, with the *antiparallel/obtuse* structure type. After the new peak appears, the original peak cannot be monitored, as the two peaks overlap significantly and the intensity of the peak for the known cocrystal increases rapidly. At the end of the experiment (after 11.4 h), only the peak for the known cocrystal is present. *Ex-situ* powder X-ray diffraction analysis of the solid phase collected at the end of the experiment confirms that the final crystallization product is a monophasic sample of the known 1,10-dihydroxydecane–(urea)$_2$ cocrystal phase with the *antiparallel/obtuse* structure type.

Summation of all ^{13}C NMR spectra recorded during the first 40 min of the crystallization experiment indicates that the transient solid form present in the early stages contains both urea and 1,10-dihydroxydecane, and the measured ^{13}C chemical shift (164.12 ppm) for urea in the transient solid form provides further insights into the possible identity of this material. First, the conventional 1,10-dihydroxydecane/urea inclusion compound (165.05 ppm) and pure solid urea (163.1 ppm) can be ruled out. However, the chemical shift for urea in the transient solid form is close to that for urea in the 1,8-dihydroxyoctane–(urea)$_2$ cocrystal (164.06 ppm), which may give a hint that the transient solid form is a 1,10-dihydroxydecane–(urea)$_2$ cocrystal with the *parallel/acute* structure type.

Clearly, the *in-situ* solid-state ^{13}C NMR results establish the crystallization conditions required to produce the new transient polymorph of the 1,10-dihydroxydecane–(urea)$_2$ cocrystal, and identify the specific 'time-window' during which this polymorph is present. Reproducing these conditions in *ex-situ* laboratory crystallization experiments therefore provides the opportunity to isolate the transient polymorph by terminating the crystallization process within the relevant time window and collecting the solid phase to allow structure determination of the new polymorph using X-ray diffraction techniques.

A subsequent study (Zhou *et al.*, 2015) showed that polymorphs of cocrystals within this family can be obtained using mechanochemical techniques. Specifically, for both 1,6-dihydroxyhexane–(urea)$_2$ and 1,8-dihydroxyoctane–(urea)$_2$, polymorphs with the *antiparallel/obtuse* structure type were obtained.

4. Combined Liquid- And Solid-State *In-situ* Crystallization NMR: 'CLASSIC NMR'

Clearly, the *in-situ* solid-state NMR strategy described above is a powerful approach for establishing the sequence of solid phases produced during crystallization and for the discovery of new polymorphs, but it gives no insights into the changes that occur in the liquid component of the crystallization system as crystallization proceeds. Importantly, knowledge of the evolution of the liquid phase during crystallization, in conjunction with knowledge of the evolution of the solid phase, has the potential to yield a significantly deeper understanding of the crystallization behaviour. To address this issue, our most recent *in-situ* NMR technique exploits the fact that a solid-state NMR spectrometer can study *both* the liquid phase *and* the solid phase in a heterogeneous solid/liquid system *using the same instrument*. By alternating between two different pulse sequences, solid-state and liquid-state NMR spectra are recorded successively, yielding essentially simultaneous information on the time-evolution of both the solid phase and the liquid phase during the crystallization process (Fig. 5). This strategy is called 'CLASSIC' NMR (Combined Liquid- And Solid-State *In-situ* Crystallization NMR). Significantly, the CLASSIC NMR experiment can be carried out on any standard solid-state NMR spectrometer, without requiring modification of the instrumentation. The key requirement is that one pulse sequence is selective for

detecting a signal from the solid phase (ideally with the liquid phase 'invisible' to the measurement) and the other pulse sequence is selective for detecting a signal from the liquid phase (ideally with the solid phase 'invisible' to the measurement). Clearly, the details of the specific pulse sequences selected for the solid-state and liquid-state measurements may depend on the specific system under investigation.

The CLASSIC NMR experiment can elucidate the complementary changes that occur in the solid and liquid phases as a function of time. Thus, the solid-state component of the CLASSIC NMR data reveals the changes in the amount and polymorphic identity of the solid phase as a function of time, as described in §3. As crystallization proceeds, the solution phase becomes more dilute and the consequent changes in solution-state speciation and the modes of molecular aggregation in solution are monitored as a function of time from the liquid-state component of the CLASSIC NMR data.

The advantages of the CLASSIC NMR strategy were first demonstrated (Hughes *et al.*, 2014) in a study of the crystallization of *m*-aminobenzoic acid (*m*-ABA) from dimethyl sulfoxide (DMSO). As described in §3.1, there are five known polymorphs of *m*-ABA, with each polymorph uniquely distinguished by its high-resolution solid-state ^{13}C NMR spectrum, enabling the polymorphs present during *in-situ* crystallization experiments to be readily identified. In the CLASSIC NMR study of the crystallization of *m*-ABA from DMSO, high-resolution solid-state ^{13}C NMR spectra were recorded using ^{1}H→^{13}C CP with high-power ^{1}H decoupling, allowing selective detection of the signal only from the solid phase. Liquid-state ^{13}C NMR spectra were recorded using a direct-excitation ^{13}C NMR pulse sequence, with no ^{1}H decoupling and with a relatively short recycle delay (of the magnitude typically used to record liquid-state NMR spectra). The absence of ^{1}H decoupling and the short recycle delay ensure that no significant signal is detected from the solid phase. The solution of *m*-ABA in DMSO was first held at 393 K for 1 h to ensure complete dissolution, then cooled over *ca* 15 min to 306 K. The CLASSIC NMR strategy was then applied for a total time of 15 h. The time to record each solid-state ^{13}C NMR spectrum was 38.4 min and the time to record each liquid-state ^{13}C NMR spectrum was 6.4 min, giving an overall time resolution of 44.8 min for the *in-situ* study. In extensive *ex-situ* tests of the crystallization of *m*-ABA from DMSO under normal laboratory conditions, only Form I was observed as the final crystallization product.

The evolution of the solid-state component of the CLASSIC ^{13}C NMR data is shown in Fig. 6(*a*). The first solid-state signal emerges *ca* 2 h after commencing the experiment, signifying the start of crystallization. From the ^{13}C chemical shifts, the solid phase is assigned as Form I. The total integrated intensity in the solid-state ^{13}C NMR spectrum then increases monotonically with time (Fig. 6*b*), indicating an increase in the amount of solid, levelling off at *ca* 8 h. No change in the solid-state ^{13}C chemical shifts is observed with time, indicating that only Form I is present during the crystallization process and no polymorphic transformation occurs within the duration of the experiment. The liquid-state ^{13}C NMR spectrum contains sharp peaks for each of the seven ^{13}C sites in the *m*-ABA molecule and only the *J*-coupling to directly bonded ^{1}H nuclei is resolved. Time-dependent changes in the concentration of *m*-ABA in the solution phase can be monitored from the changes in the total integral of the peaks for *m*-ABA in the liquid-state component of the CLASSIC ^{13}C NMR data. As shown in Fig. 6(*b*), this integral is constant until the time (*ca* 2 h) at which the first signal is observed in the solid-state ^{13}C NMR spectrum. The total

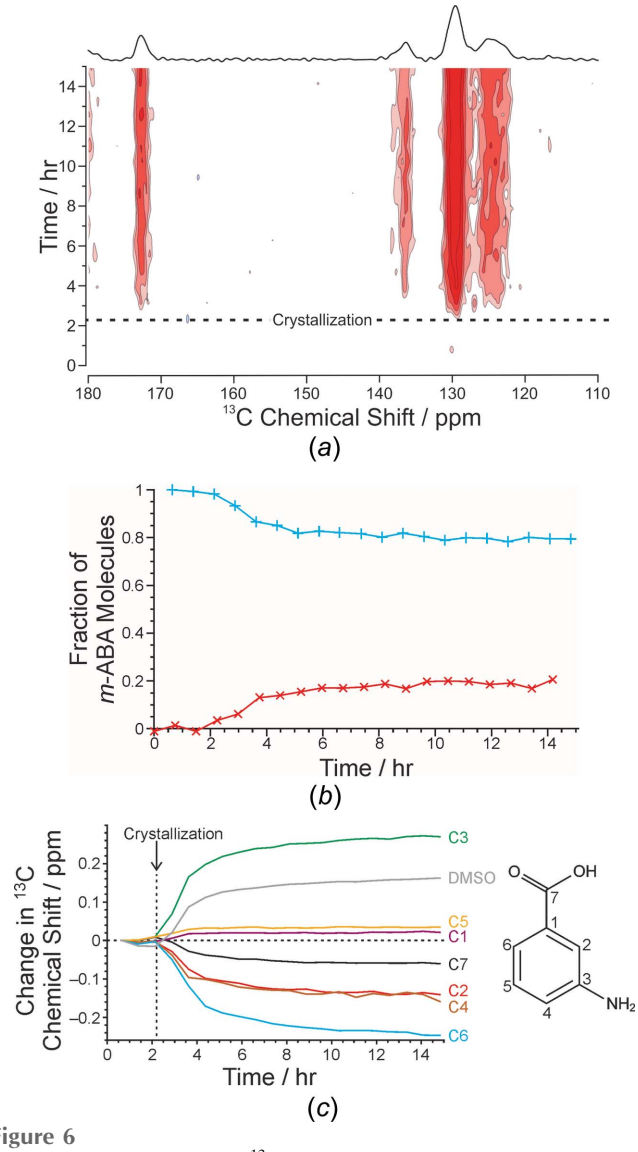

Figure 6
Results from the CLASSIC ^{13}C NMR study of crystallization of *m*-ABA from DMSO. (*a*) The solid-state component of the CLASSIC ^{13}C NMR data; the sum of all spectra (shown at the top) is identified as Form I of *m*-ABA, with no evidence that any other polymorph is present at any time during the crystallization process. (*b*) Fraction of *m*-ABA molecules in the liquid (blue; + marks) and solid (red; × marks) phases as a function of time, established from the integrals of the liquid-state and solid-state components of the CLASSIC NMR data, respectively. (*c*) The evolution of ^{13}C chemical shifts in the liquid-state component of the CLASSIC ^{13}C NMR data; the vertical dashed line indicates the time at which crystallization commenced – see part (*a*).

integral then decreases with time, before reaching a constant value at *ca* 8 h.

More details concerning the changes in the liquid phase can be gained by considering changes in the peak positions in the liquid-state ^{13}C NMR spectrum as a function of time. Fig. 6(*c*) shows the ^{13}C chemical shift for each ^{13}C site in *m*-ABA as a function of time relative to its initial value. At the start of the experiment, the system is a supersaturated solution. After crystallization begins, the supersaturation decreases and, by the end of the crystallization process, the system is an equilibrium saturated solution. From independent studies (Van Blaricom & Gilbert, 1939), it is known that *m*-ABA exists in the nonzwitterionic form in equilibrium saturated solutions in DMSO. From this knowledge, and by rationalizing the change in the chemical shift for each ^{13}C site in *m*-ABA observed as a function of time, significant insights can be gained into the nature of the supersaturated solution that exists at the start of the crystallization experiment.

As discussed in the original paper (Hughes *et al.*, 2014), the observed changes in the liquid-state ^{13}C chemical shifts as a function of time during crystallization point to the conclusion that, relative to a saturated solution of *m*-ABA in DMSO, the supersaturated solution of *m*-ABA in DMSO at the start of the crystallization experiment has (*a*) a higher proportion of zwitterionic *m*-ABA molecules and/or (*b*) a higher proportion of nonzwitterionic *m*-ABA molecules present in hydrogen-bonded aggregates (in which the NH_2 group acts as a hydrogen-bond acceptor). Both scenarios represent an increased degree of protonation of the NH_2 group of *m*-ABA, leading to increased positive charge on the N atom and promoting the specific changes in ^{13}C chemical shifts observed. Although the crystal structure of Form I of *m*-ABA has not yet been determined, it is known (Williams *et al.*, 2012) from N(1s) XPS studies that the *m*-ABA molecules are zwitterionic and clearly either situation (*a*) or (*b*) is a plausible solution-state precursor to the $O^-\cdots H-N^+$ hydrogen bonds that must exist between *m*-ABA zwitterions in the crystal structure of Form I. Although it is not possible from the available evidence to distinguish whether the system is described predominantly by situation (*a*) or (*b*), the conclusions from the CLASSIC NMR study nevertheless give clear insights into the nature of the speciation and interactions that exist in the supersaturated prenucleation solution of *m*-ABA in DMSO prior to crystallization, relative to those in the equilibrium saturated solution at the end of the crystallization process.

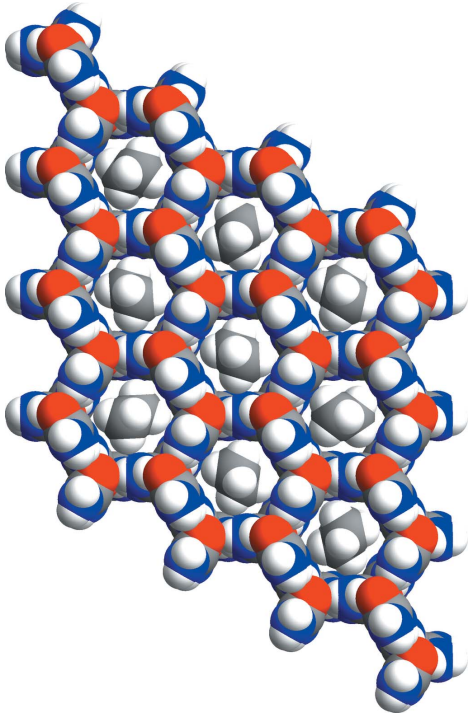

Figure 7
The crystal structure of a urea inclusion compound, viewed along the direction of the one-dimensional tunnels in the urea 'host' structure and showing *n*-alkane 'guest' molecules within the tunnels.

Furthermore, the change in the ^{13}C chemical shift for the DMSO solvent as a function of time during the crystallization process can be rationalized in a straightforward manner. As DMSO has no hydrogen-bond donor group, the only strong hydrogen bonds that DMSO can form are hydrogen bonds involving *m*-ABA as the donor and DMSO as the acceptor. As the concentration of *m*-ABA decreases during the crystallization process, there must be a corresponding decrease in the proportion of DMSO molecules engaged as acceptors in hydrogen bonds with *m*-ABA molecules, resulting in the observed ^{13}C chemical shift of DMSO becoming progressively more positive as a function of time.

We now consider a second example (Hughes *et al.*, 2015) of the application of *in-situ* NMR to probe simultaneously the evolution of both the solid and liquid phases during crystallization, focusing on the formation of urea inclusion compounds (Fetterly, 1964; Harris, 1993, 1996, 1997, 2007; Guillaume, 1999; Hollingsworth, 2002) containing long-chain *n*-alkane and α,ω-dibromoalkane guest molecules. Specifically, we discuss a CLASSIC NMR study of crystallization from a solution of urea, 1,8-dibromooctane and tetradecane (with an approximate molar ratio of 10:1:2) in methanol, with the aim of exploring the competitive inclusion of tetradecane *versus* 1,8-dibromooctane guest molecules in the urea host tunnel structure (Fig. 7) during crystal growth. The solution was prepared at 323 K, then cooled to 293 K at a constant rate over 11 h and then maintained at 293 K for a further period of several hours. Direct-excitation ^{13}C NMR spectra were recorded (with ^{1}H decoupling) throughout the cooling process and for 6 h after reaching 293 K. In contrast to most organic solids, the guest molecules in urea inclusion compounds undergo very rapid reorientational motion inside the urea host tunnel; consequently, direct-excitation ^{13}C NMR spectra recorded under conditions normally used to record liquid-state ^{13}C NMR spectra also detect a signal from the guest molecules in the solid. Thus, the direct-excitation ^{13}C NMR spectra recorded in the *in-situ* study contain signals from 1,8-dibromooctane and tetradecane molecules *both* in the solid urea inclusion compound *and* in the liquid phase. In contrast, ^{1}H$\rightarrow$^{13}C CP measurements are found to give much weaker signals for the guest molecules in the urea inclusion compounds. For this reason, only direct-excitation ^{13}C NMR

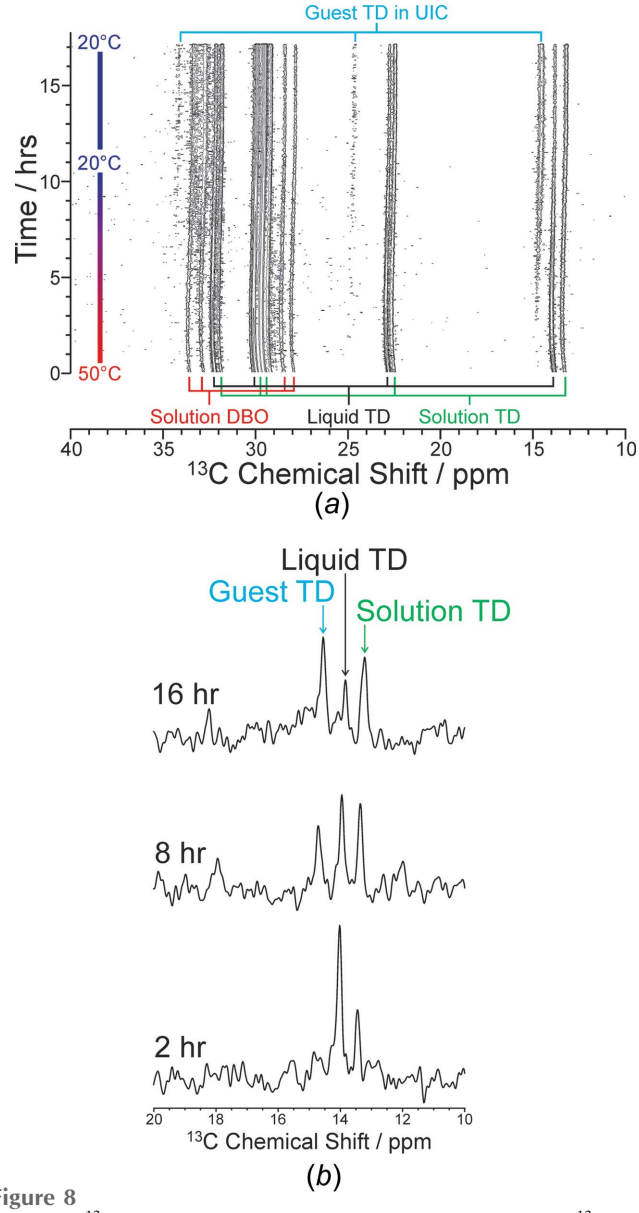

Figure 8
(*a*) *In-situ* ^{13}C NMR spectra recorded using the direct-excitation ^{13}C pulse sequence during crystallization of a urea inclusion compound (UIC) from a solution containing urea, 1,8-dibromooctane (DBO) and tetradecane (TD) in methanol. Peaks for the DBO and TD molecules in different phases are labelled. In addition to the solution phase and the solid (urea inclusion compound) phase, a pure liquid tetradecane phase is also present. The temperature of the solution as a function of time is shown at the left side. (*b*) Individual ^{13}C NMR spectra recorded at 2, 8 and 16 h, showing the region containing isotropic peaks for the methyl groups of TD molecules in different phases within the crystallization system.

spectra were recorded in this *in-situ* study of the crystallization system (Fig. 8), allowing the evolution of both the solid phase and the liquid phase to be monitored as a function of time.

Peak assignments in the *in-situ* ^{13}C NMR spectra (Fig. 8) are made by reference to spectra recorded for samples of solid urea inclusion compounds and solutions containing the individual components prepared independently. At the start of the *in-situ* crystallization experiment (at 323 K), it is clear from the ^{13}C NMR data that both 1,8-dibromooctane and tetradecane are present (together with urea) in the methanol

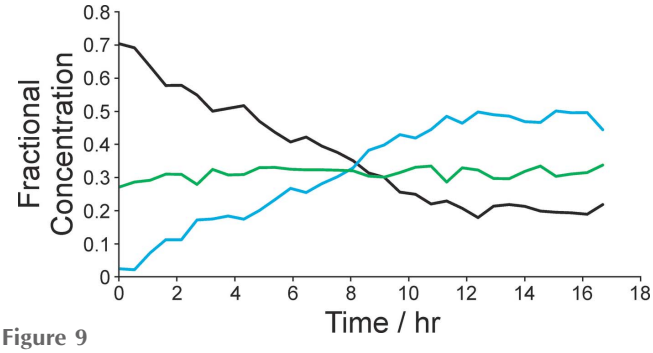

Figure 9
Time-dependence of the relative amounts of tetradecane molecules in the three distinct phases present in crystallization of tetradecane, 1,8-dibromooctane and urea from methanol, determined from the intensities of the methyl peaks in the *in-situ* ^{13}C NMR spectra (blue: guest molecules in the urea inclusion compound; green, solution phase; black, pure liquid tetradecane).

solution; however, another set of peaks is also observed, assigned to a separate liquid phase of pure tetradecane, which arises from only partial dissolution of tetradecane in methanol under the conditions of the experiment. On cooling the system, the amount of pure liquid tetradecane diminishes and, concomitantly, new peaks emerge in positions characteristic of tetradecane guest molecules in the solid urea inclusion compound. Significantly, no peaks are present for 1,8-dibromooctane guest molecules in the solid urea inclusion compound, indicating that inclusion of tetradecane guest molecules within the urea tunnel structure dominates over inclusion of 1,8-dibromooctane guest molecules. Indeed, it is well established (Harris *et al.*, 1999; Palmer *et al.*, 2013) that inclusion of any *n*-alkane longer than undecane (such as tetradecane) is energetically favoured over inclusion of 1,8-dibromooctane as the guest component in urea inclusion compounds.

Fig. 9 shows the relative amounts of tetradecane in the three different phases as a function of time during the crystallization process, established from the intensities of the ^{13}C resonances for the methyl groups of tetradecane in the three different phases. The amount of tetradecane dissolved in the methanol solution phase remains essentially constant throughout the experiment, whereas the amount of pure liquid tetradecane decreases and the amount of tetradecane in the solid phase (the urea inclusion compound) increases. It is clear that crystallization of the urea inclusion compound containing tetradecane guest molecules occurs in the solution phase. However, while tetradecane molecules are consumed from the solution phase by the crystallization process, the partitioning of tetradecane between the solution phase and the pure liquid phase adjusts in order to maintain an essentially constant concentration within the solution phase, leading to a decrease in the amount of the pure liquid tetradecane phase as a function of time. Significantly, the *in-situ* ^{13}C NMR data reveal clearly that the decrease in the amount of the pure liquid tetradecane phase as a function of time exactly mirrors the rise in the amount of tetradecane in the solid phase.

We emphasize that the complexity of this three-phase crystallization system has been revealed through a combined

liquid-state and solid-state *in-situ* NMR study in which the same NMR measurement technique was suitable for observing the two liquid phases present and the solid phase, with the three distinct phases distinguished simply on the basis of isotropic chemical shifts. To study the crystallization behaviour of materials in which the molecules undergo rapid dynamics, this type of implementation of the CLASSIC NMR strategy is likely to prove very successful. However, in the more common situation in which the relevant spin-lattice relaxation times for the solid phase are substantially longer than those for the liquid phase, the original implementation of the CLASSIC NMR strategy (Hughes *et al.*, 2014) in which the *in-situ* experiment is carried out using two alternating pulse sequences, allowing the alternate (and selective) measurement of liquid-state and solid-state NMR spectra, is likely to be the most appropriate approach for gaining insights into the complementary evolution of each phase within the crystallization system.

5. *In-situ* liquid-state NMR studies of crystallization processes

In some cases, long $T_1(^1H)$ or $T_1(^{13}C)$ relaxation times for organic solids are such that the recycle delay required to record solid-state ^{13}C NMR spectra using $^1H \rightarrow {}^{13}C$ CP or ^{13}C direct excitation, respectively, are prohibitively long and would not constitute an acceptable time-resolution for monitoring crystallization processes, especially when the crystallization process is relatively rapid. In such cases, however, liquid-state ^{13}C NMR spectra can still be recorded quickly [as $T_1(^{13}C)$ relaxation times for the liquid phase are significantly shorter] and may still yield significant insights into the evolution of the crystallization system as a function of time.

To illustrate the utility of *in-situ* liquid-state NMR studies in such cases for which *in-situ* solid-state NMR studies are not viable, we focus on *in-situ* liquid-state ^1H NMR and ^{19}F NMR studies (Hughes *et al.*, 2015) of crystallization from a solution containing equimolar amounts of benzoic acid (BA) and pentafluorobenzoic acid (PFBA) in d_2-dichloromethane. BA and PFBA are known to form a 1:1 cocrystal material; in the crystal structure (Gdaniec *et al.*, 2003; Albesa-Jové *et al.*, 2004; Reddy *et al.*, 2004), the BA and PFBA molecules form heteromolecular pairs linked by the well-known double hydrogen-bonded carboxylic acid dimer motif, and there is alternating stacking of the phenyl and pentafluorophenyl rings of the BA and PFBA molecules.

Ex-situ crystallization experiments indicate that the known cocrystal phase is the only crystallization product from dichloromethane, but our *in-situ* liquid-state NMR studies provide significant insights concerning the time-dependence of the crystallization process. Fig. 10 shows the results from separate *in-situ* liquid-state ^1H NMR and ^{19}F NMR studies of crystallization from identical solutions of BA and PFBA (1:1 molar ratio) in d_2-dichloromethane.[3] In each experiment, there is initially no change in the liquid-state NMR spectrum as a function of time, but then a very abrupt change is observed in the chemical shifts at *ca* 38 min in the ^1H NMR data and at *ca* 10 min in the ^{19}F NMR data, corresponding to very rapid formation of the BA/PFBA cocrystal material in each case. The integrals of the ^1H NMR and ^{19}F NMR spectra as a function of time (Fig. 11) reveal a dramatic decrease in intensity at the same value of time as the abrupt changes in solution-state chemical shifts, indicating that the changes in chemical shifts are associated with a very sudden and rapid dilution of the solution phase, corresponding to a very rapid crystallization process. The existence of a lag time before crystallization and the variability in the length of this lag time in different experiments are typical in this system, which is consistent with the fact that the sudden change in chemical shifts is observed at a different time in the ^1H NMR data and the ^{19}F NMR data. Such sudden and abrupt changes in the solution state may arise, for example, when a very rare (stochastic) nucleation event in a highly supersaturated solution triggers a significant amount of rapid crystallization.

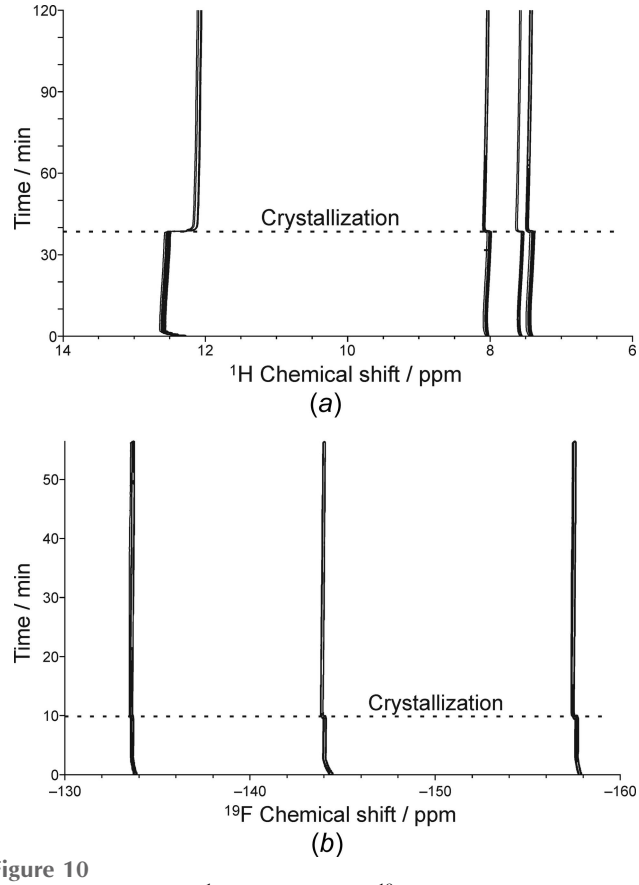

Figure 10
In-situ liquid-state (*a*) ^1H NMR and (*b*) ^{19}F NMR spectra recorded (in separate experiments) as a function of time during crystallization of benzoic acid and pentafluorobenzoic acid from d_2-dichloromethane. In each case, the dashed line represents the time at which abrupt changes are observed in the liquid-state chemical shifts, due to rapid crystallization.

In the *in-situ* liquid-state ^1H NMR data (Fig. 10), different peaks are affected in significantly different ways by the crystallization process, reflecting the rapid decrease in concen-

[3] Due to the proximity of the ^1H and ^{19}F Larmor frequencies, it is not possible to record alternate ^1H NMR and ^{19}F NMR spectra during the *same* crystallization experiment.

tration of the solution phase and the correspondingly rapid changes in the nature and relative probabilities of different intermolecular interactions involving the BA and PFBA molecules (including changes in their interactions with the solvent molecules). The abrupt change in ^{1}H chemical shift is largest for the carboxylic acid group, which shifts by *ca* −0.4 ppm, while the ^{1}H chemical shifts for the phenyl ring of BA move in the opposite direction by *ca* +0.1 ppm. The fact that only one ^{1}H resonance is observed for all the carboxylic acid groups indicates that rapid proton exchange occurs between BA and PFBA molecules in the solution phase, as well as between different interaction environments of these molecules. In the prenucleation supersaturated solution that exists before the rapid crystallization event, these interaction environments must include a range of prenucleation aggregates and clusters that could represent viable species on the pathway to nucleation. At the moment of crystallization, the change in the ^{1}H chemical shift for the carboxylic acid groups suggests that, in the supersaturated solution prior to crystallization, the proportion of molecules in solution that exist in hydrogen-bonded dimers is significantly higher than that in the more dilute solution at the end of the crystallization process (it is well established that the ^{1}H chemical shift of carboxylic acids is more positive for a hydrogen-bonded dimer than for a non-hydrogen-bonded monomer).

From a practical perspective, we emphasize that our *in-situ* liquid-state NMR measurements on crystallizing systems utilize magic-angle spinning to ensure good spectral quality. In our experience, it is preferable to use a solid-state NMR spectrometer rather than a dedicated liquid-state NMR spectrometer for such studies, as liquid-state NMR spectra recorded for solutions undergoing crystallization suffer from significant line broadening due to poor shimming when solid particles are present in the solution (*i.e.* after crystallization has commenced).

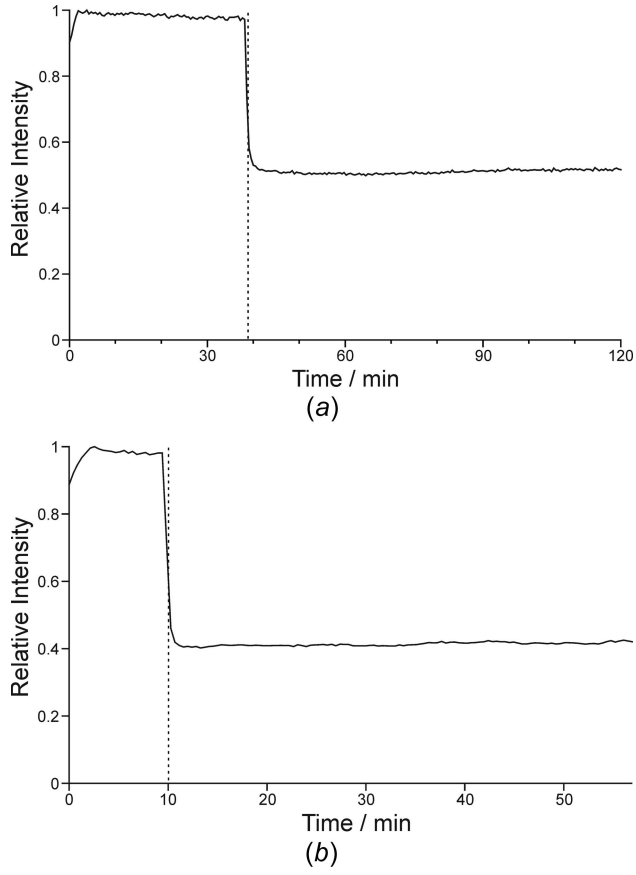

Figure 11
Peak intensities recorded as a function of time during crystallization of benzoic acid and pentafluorobenzoic acid from d_2-dichloromethane, determined from (*a*) the *in-situ* liquid-state ^{1}H NMR spectra (integral of the peak at *ca* 12 ppm) and (*b*) the *in-situ* liquid-state ^{19}F NMR spectra (integral of the peak at *ca* −134 ppm) shown in Fig. 10. In each case, the dashed line represents the time at which abrupt changes are observed in the peak intensities, due to rapid crystallization.

6. Future prospects

The *NMR Crystallization* strategies described here for probing the evolution of crystallization processes using *in-situ* NMR techniques have considerable scope and potential to provide fundamental insights into the nature of crystallization behaviour. These strategies offer new opportunities for directly monitoring the time-evolution of crystallization systems, yielding information that cannot be gained from *ex-situ* analysis of the final solid product recovered from a crystallization experiment. While we have demonstrated the merits of exploiting selective *in-situ* solid-state NMR measurements or selective *in-situ* liquid-state NMR measurements in this field, we emphasize that the recently developed CLASSIC NMR strategy extends significantly the scope and capability of both of these approaches for the *in-situ* monitoring of crystallization processes, as it is unique in providing simultaneous and complementary information on the time-evolution of *both* the solid phase *and* the liquid phase. We fully anticipate that the advantages of the CLASSIC NMR strategy in particular will yield significant new knowledge on a wide range of crystallization systems in the future.

Acknowledgements

We are grateful to the UK 850 MHz Solid-State NMR Facility for the award of significant amounts of time for *in-situ* NMR studies of crystallization processes. The UK 850 MHz Solid-State NMR Facility was funded by EPSRC and BBSRC, as well as the University of Warwick, including part funding through Birmingham Science City Advanced Materials Projects 1 and 2 supported by Advantage West Midlands and the European Regional Development Fund. Our research in the field described in this article has benefitted from discussions within the framework of the EPSRC Collaborative Computational Project in NMR Crystallography (award EP/M022501/1).

References

Ahn, S., Guo, F., Kariuki, B. M. & Harris, K. D. M. (2006). *J. Am. Chem. Soc.* **128**, 8441–8452.

Albesa-Jové, D., Kariuki, B. M., Kitchin, S. J., Grice, L., Cheung, E. Y. & Harris, K. D. M. (2004). *ChemPhysChem*, **5**, 414–418.

Albrecht, G. & Corey, R. B. (1939). *J. Am. Chem. Soc.* **61**, 1087–1103.

Apperley, D. C., Harris, R. K. & Hodgkinson, P. (2012). In *Solid State NMR: Basic Principles & Practice*. New York: Momentum Press LLC.

Balimann, G. E., Groombridge, C. J., Harris, R. K., Packer, K. J., Say, B. J. & Tanner, S. F. (1981). *Philos. Trans. R. Soc. London Ser. A*, **299**, 643–663.

Bernstein, J. (2002). In *Polymorphism in Molecular Crystals*. Oxford University Press.

Bernstein, J. (2005). *Chem. Commun.* pp. 5007–5012.

Boldyreva, E. V., Drebushchak, V. A., Drebushchak, T. N., Paukov, I. E., Kovalevskaya, Y. A. & Shutova, E. S. (2003). *J. Therm. Anal. Calorim.* **73**, 409–418.

Chen, C., Cook, O., Nicholson, C. E. & Cooper, S. J. (2011). *Cryst. Growth Des.* **11**, 2228–2237.

Chen, S., Xi, H. & Yu, L. (2005). *J. Am. Chem. Soc.* **127**, 17439–17444.

Davey, R. J. (2003). *Chem. Commun.* pp. 1463–1467.

Drebushchak, V. A., Boldyreva, E. V., Drebushchak, T. N. & Shutova, E. S. (2002). *J. Cryst. Growth*, **241**, 266–268.

Drebushchak, T. N., Boldyreva, E. V. & Shutova, E. S. (2002). *Acta Cryst.* E**58**, o634–o636.

Duer, M. J. (2004). In *Introduction to Solid-State NMR Spectroscopy*. Oxford: Blackwell Publishing Ltd.

Dunitz, J. D. (1991). *Pure Appl. Chem.* **63**, 177–185.

Ferrari, E. S., Davey, R. J., Cross, W. I., Gillon, A. L. & Towler, C. S. (2002). *Cryst. Growth Des.* **3**, 53–60.

Fetterly, L. C. (1964). *Non-Stoichiometric Compounds*, pp. 491–567. New York: Academic Press.

Garetz, B. A., Matic, J. & Myerson, A. S. (2002). *Phys. Rev. Lett.* **89**, 175501.

Gdaniec, M., Jankowski, W., Milewska, M. J. & Połoński, T. (2003). *Angew. Chem. Int. Ed.* **42**, 3903–3906.

Guillaume, F. (1999). *J. Chim. Phys. (Paris)*, **96**, 1295–1315.

Hamad, S., Hughes, C. E., Catlow, C. R. A. & Harris, K. D. M. (2008). *J. Phys. Chem. B*, **112**, 7280–7288.

Han, G. J., Thirunahari, S., Chow, P. S. & Tan, R. B. H. (2013). *CrystEngComm*, **15**, 1218–1224.

Harris, K. D. M. (1993). *J. Solid State Chem.* **106**, 83–98.

Harris, K. D. M. (1996). *J. Mol. Struct.* **374**, 241–250.

Harris, K. D. M. (1997). *Chem. Soc. Rev.* **26**, 279–289.

Harris, R. K. (2006). *Analyst*, **131**, 351–373.

Harris, K. D. M. (2007). *Supramol. Chem.* **19**, 47–53.

Harris, K. D. M., Jupp, P. E. & Lee, S.-O. (1999). *J. Chem. Phys.* **111**, 9784–9790.

Harris, K. D. M. & Thomas, J. M. (1991). *J. Solid State Chem.* **94**, 197–205.

Hollingsworth, M. D. (2002). *Science*, **295**, 2410–2413.

Hughes, C. E., Hamad, S., Harris, K. D. M., Catlow, C. R. A. & Griffiths, P. C. (2007). *Faraday Discuss.* **136**, 71–89.

Hughes, C. E. & Harris, K. D. M. (2008). *J. Phys. Chem. A*, **112**, 6808–6810.

Hughes, C. E. & Harris, K. D. M. (2009). *New J. Chem.* **33**, 713–716.

Hughes, C. E. & Harris, K. D. M. (2010). *Chem. Commun.* **46**, 4982–4984.

Hughes, C. E., Williams, P. A. & Harris, K. D. M. (2014). *Angew. Chem. Int. Ed.* **53**, 8939–8943.

Hughes, C. E., Williams, P. A., Keast, V. L., Charalampopoulos, V. G., Edwards-Gau, G. R. & Harris, K. D. M. (2015). *Faraday Discuss.* **179**, 115–140.

Hughes, C. E., Williams, P. A., Peskett, T. R. & Harris, K. D. M. (2012). *J. Phys. Chem. Lett.* **3**, 3176–3181.

Iitaka, Y. (1960). *Acta Cryst.* **13**, 35–45.

Iitaka, Y. (1961). *Acta Cryst.* **14**, 1–10.

Jönsson, P.-G. & Kvick, Å. (1972). *Acta Cryst.* B**28**, 1827–1833.

Kahr, B. & McBride, J. M. (1992). *Angew. Chem. Int. Ed.* **31**, 1–26.

Kvick, Å., Canning, W. M., Koetzle, T. F. & Williams, G. J. B. (1980). *Acta Cryst.* B**36**, 115–120.

Martí-Rujas, J., Kariuki, B. M., Hughes, C. E., Morte-Ródenas, A., Guo, F., Glavcheva-Laleva, Z., Taştemür, K., Ooi, L.-L., Yeo, L. & Harris, K. D. M. (2011). *New J. Chem.* **35**, 1515–1521.

Palmer, B. A., Le Comte, A., Harris, K. D. M. & Guillaume, F. (2013). *J. Am. Chem. Soc.* **135**, 14512–14515.

Perlovich, G. L., Hansen, L. K. & Bauer-Brandl, A. (2001). *J. Therm. Anal. Calorim.* **66**, 699–715.

Pienack, N. & Bensch, W. (2011). *Angew. Chem. Int. Ed.* **50**, 2014–2034.

Poornachary, S. K., Chow, P. S. & Tan, R. B. H. (2007). *Cryst. Growth Des.* **8**, 179–185.

Price, S. L. (2008). *Acc. Chem. Res.* **42**, 117–126.

Reddy, L. S., Nangia, A. & Lynch, V. M. (2004). *Cryst. Growth Des.* **4**, 89–94.

RSC (2007). *Crystal Growth and Nucleation*, Vol. 136, *Faraday Discussions*. London: Royal Society of Chemistry.

Taylor, R. E. (2004). *Concepts Magn. Reson.* **22A**, 79–89.

Théorêt, A. (1971). *Spectrochim. Acta Part A*, **27**, 11–18.

Towler, C. S., Davey, R. J., Lancaster, R. W. & Price, C. J. (2004). *J. Am. Chem. Soc.* **126**, 13347–13353.

Van Blaricom, L. & Gilbert, E. F. (1939). *J. Am. Chem. Soc.* **61**, 3238–3239.

Voogd, J., Verzijl, B. H. M. & Duisenberg, A. J. M. (1980). *Acta Cryst.* B**36**, 2805–2806.

Weissbuch, I., Torbeev, V. Y., Leiserowitz, L. & Lahav, M. (2005). *Angew. Chem. Int. Ed.* **44**, 3226–3229.

Williams, P. A., Hughes, C. E., Lim, G. K., Kariuki, B. M. & Harris, K. D. M. (2012). *Cryst. Growth Des.* **12**, 3104–3113.

Xu, M. & Harris, K. D. M. (2007). *J. Phys. Chem. B*, **111**, 8705–8707.

Zhou, Y., Guo, F., Hughes, C. E., Browne, D. L., Peskett, T. R. & Harris, K. D. M. (2015). *Cryst. Growth Des.* **15**, 2901–2907.